Applied Physics A (2021) 127:585
https://doi.org/10.1007/s00339-021-04734-z

Applied Physics A
Materials Science & Processing

Effect of characterization probes on the properties of graphene oxide and reduced graphene oxide

Apurva Sinha[1] · Pranay Ranjan[1,2,3] · Ajay D. Thakur[1]

Received: 17 May 2021 / Accepted: 30 June 2021 / Published online: 7 July 2021

Abstract

Graphene Oxide (GO) has tremendous application potential as a functional material. However, we found GO to be extremely sensitive toward external energy in the form of heat, light, X-rays, etc. It is because the Oxygen Functional Groups (epoxide, carbonyl, carboxyl, hydroxyl, etc.) attached to the underlying monomolecular layer of carbon in GO are prone to reduction through externally supplied energy leading to the formation of reduced Graphene Oxide (rGO). Eventually, GO lacks preserving its original chemical composition, physical and chemical properties while interacting with the measurement probes. In addition, GO also undergoes a gradual reduction over a period in an ambient environment. This obvious behavior of GO compelled us to re-examine the related literature. In this report, we studied the detailed effects of various characterization tools, possible ways to minimize the side-effects while measurement, and an alternative way to use GO for its various uses. This involved the review of not only the different important parameters of the characterizing probes but also its synthesis protocols and the environment of its storing desiccator. In this direction, we report a careful set of experiments using X-ray Diffraction, X-ray Photoemission Spectroscopy, Raman Spectroscopy, UV–Visible Spectroscopy, Photoluminescence Spectroscopy, Transmission Electron Microscopy and Atomic Force Microscopy. This elucidates the precautions needed while establishing the best practices in GO synthesis and characterization for addressing the exact functional requirements related to an end application. Also, we did a similar study for reduced Graphene Oxide (rGO).

Keywords Graphene oxide · Reduced graphene oxide · Ambient environment · Chemical properties · X-ray photo spectroscopy

1 Introduction

Chemical exfoliation of graphite leads to the formation of graphene oxide (GO). The Oxygen Functional Groups (OFGs) (e.g., epoxide, carbonyl, carboxyl, hydroxyl, etc.) attached to the underlying monomolecular layer of carbon in GO is responsible for its exotic multifunctional nature. Reduction of GO provides a cost-effective route for the production of single-layer graphene-like material. Besides this, GO also possesses unique electrical [1], mechanical [2], optical [3, 4] and chemical [5] properties due to the presence of these OFGs [1]. OFGs enable GO to become water-soluble which eases its deposition on a substrate through drop casting, spin-coating, Langmuir Blodgett techniques and opens up routes for cost-effective graphene-based devices [1, 6]. OFGs also aids in the selective functionalization of GO including the attachment of polymers, various organic species and biological species. On reduction of GO to reduced graphene oxide (rGO), its electrical property changes from an insulator to a semiconductor/semi-metal through the restoration of π networks [7]. These unique properties of GO lead to its application in the field of electronics [7], energy [8], environmental remediation [9] and biomedicine [10]. Some of the laboratory-scale demonstrations of GO in the field of environmental sensing and biological application involve environmental sensing [9, 11], water decontamination [12], solar desalination [13], antibacterial coatings [14],

Apurva Sinha and Pranay Ranjan have contributed equally.

✉ Ajay D. Thakur
ajay.thakur@iitp.ac.in

[1] Department of Physics, Indian Institute of Technology Patna, Bihta 801106, India

[2] Department of Physics, United Arab Emirates University, Al-Ain 15551, UAE

[3] National Water and Energy Center, United Arab Emirates University, Al-Ain 15551, UAE

photo-thermal cancer therapy [15], drug delivery [15] and accelerated differentiation of neural stem cells [16]. Moreover, GO also finds application in the field of microwave absorption [17], energy [8, 18], optoelectronics [19] and tribology [20]. Historically, the synthesis of GO was first reported by Brodie et al. [21] in 1859 followed by the series of efforts by Gottschalk et al. [22], Staundenmaier et al. [23], Berthelot et al. [24], Luzi et al. [25], Charpy et al. [26], Hamdy et al. [27], Weinschenk et al. [28], Kohlschütter and Haenni et al. [29], Hummers and Offeman et al. [30], Hirata et al. [31], Marcano's et al. [6]. The continued efforts in this direction point to the interest in the science behind oxidative exfoliation that leads to the formation of GO.

A cursory look at the properties of GO reported in literature shows a considerable variation (see Table 1). Surprisingly, the characteristic signatures obtained for GO using a host of characterization techniques including X-ray Diffraction (XRD), Raman Spectroscopy, High Resolution Transmission Electron Microscopy (HRTEM), Selective Area Electron Diffraction (SAED), Photoluminescence (PL) studies, UV–Visible (UV–Vis) absorption spectroscopy and X-ray Photoemission Spectroscopy (XPS) varies significantly across literature reports. XRD is the basic technique to determine the phase formation and any variation from the signature peak raises concern and question about the formation of materials and the phase purity. However, in the case of GO, the observed variation in the characteristic 2θ peak corresponds to a variation in the corresponding lattice spacing (d) by several Angstroms. Poh et al. [32], Shen et al. [40] and Peng et al. [44] reported d as 7.08 Å, 7.26 Å and 7.8 Å, respectively, which signifies a lower degree of oxidation in comparison to the observations by Hirata et al. [31], Marcano et al. [6], Shen et al. [40], Peng et al. [44] and Ranjan et al. [47] where d was reported in the range of 8.13–9.74 Å.

Table 1 Comparison of GO signature reported through various experimental techniques in the literature

Sl	XRD	Raman shift (cm^{-1})		UV–Vis Abs	Binding energies from XPS (eV)				
	d (Å)	G band	D band	Peak (nm)	C–C /C = C	C = O	C–O	C–OH	O–C–OH
1	7.08 Å [32]	1560	1350 [32]	231 [35]	284.8	287.8	286.2 [33]	–	–
2	8.13 Å [32]	1585	1350 [34]	230 [36]	284.6	288.5	286.6 [34]	–	–
3	8.3 Å [31]	1590	1350 [6]	227 [38]	284.8	287.8	286.2 [6]	–	–
4	9.5 Å [6] 9.0 Å [6] 8.0 Å [6]	1582.36, 1584.1	1350 [37]	229 [42]	284.4	288	285.3 [39]	–	–
5	7.26 Å [40]	1580	1340 [41]	232 [42]	284.5, 284.8	287.8	286.2 [43]	–	–
6	7.8 Å [44]	1600	1353 [44]	233 [42]	284.8	287.8	286.2 [45]	–	–
7	9.0 Å [44]	1592	1348 [39]	235 [48]	284.4	286.7	–	285.7	288 [46]
8	9.74 Å [47]	1593	1352 [38]	227.5 [36]	284.6	288.3	286.5 [12]	–	–
9	–	1594	1363 [45]	–	284.5	287.8	286.4	–	289 [49]
10	–	1585	1330 [50]	–	284.5	288	–	287 [20]	–
11	–	1598	1357 [51]	–	284.6	288.3	286.5 [52]	–	–
12	–	1580	1350 [53]	–	285	287.8–288	286.8–287	–	289–289.3 [54]
13	–	–	–	–	285	287.7	–	286	289.2 [50]
14	–	–	–	–	284.3	288.8	285.6 [51]	–	–
15	–	–	–	–	285	288.3	–	–	289.4 [55]
16	–	–	–	–	284.6	287	288.5 [56]	–	–
17	–	–	–	–	286.6	287.9	286.6 [52]	–	–
18	–	–	–	–	284.4	288.4	286.6	–	289.8 [57]
19	–	–	–	–	284.5–285	288	286.5	–	289.5 [57]
20	–	–	–	–	284.5–285.4	–	286.5	–	288.9, 290.4 [58]
21	–	–	–	–	285	288.2	287 [59]	–	–
22	–	–	–	–	284.8	287.1	–	286.2	288.8 [60]
23	8.3 Å [82]	1580, 1595, 1600 [82]	1350, 1415 [82]	231 [82]	–	–	–	–	–
24	7.7 Å [83]	–	–	230 [83]	–	–	–	–	–
25	8.1 Å [84]	–	–	228 [84]	–	–	–	–	–
26	–	1581	1352 [85]	–	286.2 /284.9	288.7	288.3 [85]	–	–
27	8.3 Å [86]	–	–	–	–	288.2	286.7	–	289.4 [86]

This may arise due to the variation in the degree of oxidation as stacked GO layers contain *n* number of OFGs and need to be documented carefully. Raman spectroscopy is a widely used non-invasive technique for differentiating between GO, rGO, graphene and amorphous carbon. GO spectra mainly consist of three major peaks named as D peak near 1300 cm^{-1}, G peak near 1600 cm^{-1} and the 2D peak near 2600 cm^{-1}. From Table 1, we can note the variability in the location of D- and G-peaks for GO. Here it is crucial to understand the role of the light source (used for obtaining the Raman spectra) in the process of reduction (leading to detachment of OFGs). Poh et al. [32] reported D- and G-peaks of GO at 1350 cm^{-1} and 1560 cm^{-1}, respectively. However, reports by Marcano et al. [6], Eigler et al. [41], Stankovich et al. [45], etc., differ among themselves on this. In the case of UV–Vis spectra of GO, the π–π^* transition is ascribed to the C = C bond. Peng et al. [36] observed the π–π^* peak at 230 nm, Johra et al. [48] at 235 nm while other reports (see Table 1) for the π–π^* transition lie in the range 227.5–233 nm. Interestingly, this can also arise from the modifications in OFG fraction that may result from steps followed during sample preparation for a UV–Vis absorption study (e.g., the concentration of GO solution, ultrasonication details, etc.). Reports from another crucial characterization technique i.e., XPS studies also show variations in the binding energies corresponding to different functional group. Dreyer et al. [33], Tao et al. [34], Chu et al. [39] and others considered the de-convolution of C1s into C–C/C = C, C–OH, O–C–O/C = O, C–O and found their positions in the range of 283.8–285 eV, 285.7–287 eV, 288–290.4 eV, 285.3–288.5 eV as shown in Table 1. It may be due to the differences in the screening as well as charging effect, sample mounting methods and scan rates. Differences in scan rates can also lead to the reduction of GO and need careful investigation. Our work deals with the above caveats and attempts to bring out the role of sample preparation details and the conditions during characterization. This in turn is expected to lead to a better understanding of GO and its derivatives and also help in making a judicious choice of these materials for various applications.

2 Experimental details

2.1 Synthesis details

The chemicals (of analytical grade) procured from Alfa-Aesar and Sigma Aldrich are used without any further treatment and purification. Parent GO sample was prepared using a modified Hummers method reported earlier [47]. Graphite flakes (C) (mesh size 100) and Potassium permanganate ($KMnO_4$) were crushed in a mortar and pestle for 10 min in a ratio of 1:6. The mixture of C: $KMnO_4$ was cooled at 5 °C for 6 h in a refrigerator. An acid mixture of sulfuric acid (H_2SO_4–99.99%) and orthophosphoric acid (H_3PO_4–85%), in the ratio of 9:1, was prepared in a separate beaker and was cooled at 5 °C for 6 h. The two separate mixtures of C: $KMnO_4$ and H_2SO_4: H_3PO_4 were mixed in a separate beaker, and the temperature of the beaker was elevated to 65 °C (for the sample labeled GO-65C) and 50 °C (for the sample labeled GO-50C) with constant stirring for 24 h. The reaction was then allowed to cool at room temperature, and deionized water (DI water) ice of 600 ml was added to the solution followed by 7 ml addition of H_2O_2 (30% w/w). The resulting mixture was centrifuged at 10,000 rpm for 5 min followed by successive washing by water (twice), ethanol (thrice) and HCl (37%) (once). The obtained material is GO gel which is vacuum dried for 8 h to get GO foam followed by crushing in mortar and pestle to obtain GO powder. rGO has been prepared as per the already reported protocol [61]. We dispersed GO flakes in 300 ml of DI water and sonicated to get a homogenous solution. After sonication for 2 h, 1 M sodium hydroxide (NaOH) was added and stirred for 1 h followed by dropwise addition of L-ascorbic acid (LAA) solution in DI water (1:10). After the LAA addition is completed, the temperature of the mixture is raised to 95 °C. rGO samples with different degrees of reduction are prepared by decanting the required amount at different times, T_{Decant}. Washing is done first using DI water diluted 35% hydrochloric acid (1:1) (1 time) and DI water (2 times). The washed samples are then desiccated for 5 h to obtain the dried rGO samples. We label the rGO samples reported in this paper based on T_{Decant} (rGO-01 min, rGO-60 min and rGO-80 min for T_{Decant} of 1 min, 60 min and 80 min, respectively).

2.2 Details of characterization techniques

XRD data of the samples were obtained using Rigaku TTRX-III diffractometer with 1.54 Å Cu–Kα X-ray source. A Jeol JEM-2100 transmission electron microscope was used for obtaining SAED patterns. A confocal micro-Raman spectrometer from Seki-Technotron corporation, Japan with 514.5 nm Argon ion laser has been used for the Raman studies. Perkin Elmer Lambda-35 UV–Vis spectrophotometer was used to study UV–Vis spectroscopy. We used Spex-FluoroMax-3 spectrofluorimeter for Photoluminescence study. XPS studies of the as-prepared GO powder were done with the help of ESCA + Omicron Nano-technology GmbH. Atomic Force Microscopy (AFM) Agilent 5500 was used for obtaining the morphological structure of the GO films. The exact measurement conditions used for specific equipment are mentioned in the Results and Discussions section, wherever applicable.

3 Results and discussion

3.1 Sample dependent XRD peak positions of GO and rGO

We investigate the phase purity of the as-synthesized GO sample using X-ray diffraction (XRD). A peak centered at $2\theta = 9.74°$ corresponding to [002] plane (see Fig. 1a) is observed suggesting a high degree of intercalation of OFGs. Moreover, the absence of any other peak, especially near $2\theta = 26°$ reveals absence of any graphitic impurity. Hence, the as-synthesized GO is in its pure phase as reported elsewhere [47]. We now focus on certain factors that affect the nature of the sample and hence lead to observable changes in the XRD pattern. We measured the diffraction pattern of GO-65C treated at different temperatures (room temperature, 100° C, 200° C and 300° C) (see Fig. 1a, b, c and d). We observed that the peak at 9.74° in as-synthesized GO-65C goes over to a broad hump centered near 26° as we raised the temperature. This happens effectively due to the removal of OFGs. At 100° C, it can be observed that there starts an emergence of a hump near 26° (signature of rGO), which becomes prominent at 200° C. However, the signature of GO is still present at 200 °C near 9.74°, indicating an incomplete reduction of GO. At 300 °C, the signature peak for GO completely vanishes hinting at the removal of OFGs. Figure 1e summarizes the measured sheet resistance values of the samples heated at different temperatures. To measure their resistance values, we prepared four different samples using a quartz glass substrate. GO-65C films were deposited uniformly on each of them using a spin-coater. After deposition, one of them was kept at room temperature as a reference sample in a desiccator. And other three samples were prepared by heating them individually at 100℃, 200℃ and 300℃, respectively, in a vacuum oven for 2 h each. Further, we employed a four-probe method to measure the resistance value of each of the samples. We observed that the sheet resistance of the GO sample heated till 200 °C remains high (~MΩ) but suddenly falls to a low value on further heating (~kΩ). We surmise that even a small fraction of GO leads to an insulating behavior of the film (as seen in Fig. 1e). We also did Scanning Electron Micrography (SEM) of all the four samples (shown in Fig. S2) and studied the changes in the morphology of the GO sheets after heating at 100℃, 200℃ and 300℃, respectively. We next explore the shelf life of GO with the aim at evidencing the precautions required in its long-term storage (in a typical desiccated environment). Reduction in GO sample as a function of time clearly revealed that GO can deteriorate even in a dark evacuated desiccator (see Fig. 1f, g and h). Apart from the peak of GO at 9.74° (Fig. 1f), a broad hump developed near 26° after 2 and 6 months of preservation in Fig. 1g and h, respectively, marks the partial reduction of GO over the period. The cause may be attributed to its acidic nature [62] and the vacuum degradation with the time elapsed. Since GO being hydrophilic in nature readily

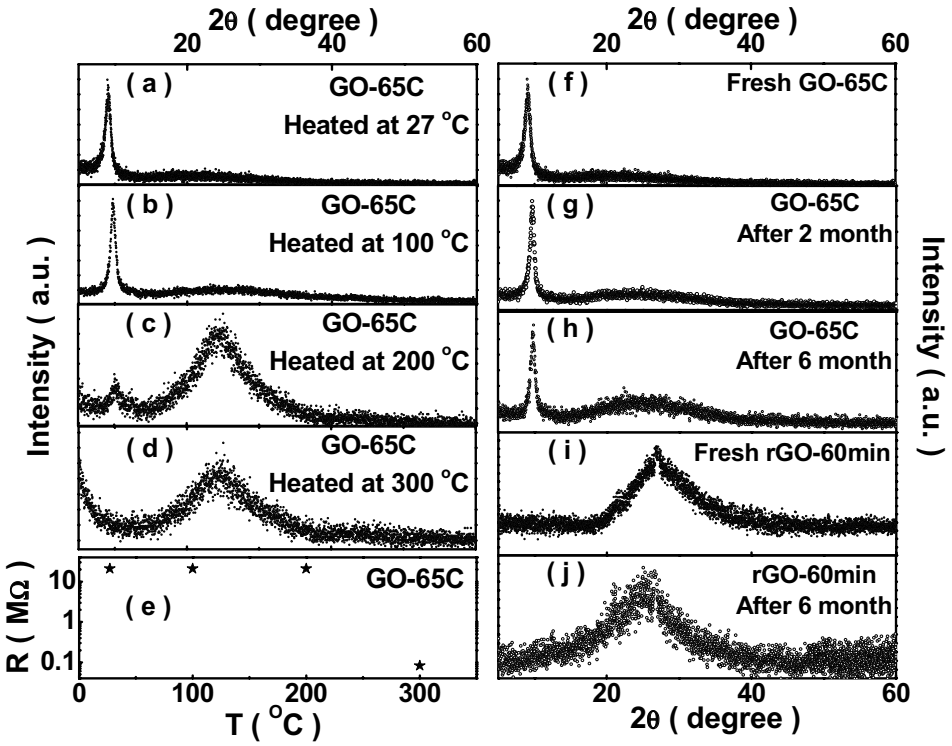

Fig. 1 XRD pattern of GO-65C heated at different temperatures (panels (**a**)–(**d**)); XRD pattern for GO-65C and rGO-60 min at different times (panels (**f**)–(**j**)); Resistance of the thermally reduced GO-65C as a function of reduction temperatures (panel (**e**))

traps the moisture content from the surrounding due to gradual vacuum degradation and the interaction may leads to the deterioration of GO. On the other hand, there is negligible change in the XRD pattern of rGO (see Fig. 1i and j; here we use the 1 h reduced rGO i.e., rGO-60 min using the chemical reduction method as elucidated above). Thus, time and temperatures must be monitored carefully to ensure the quality of GO, and the same can be quickly evaluated using XRD. If storage is desirable for future applications, we recommend storing rGO instead of GO.

3.2 Care related to interpretation of TEM and SAED for GO

GO contains OFGs that are prone to reduction by supplying external energy (such as exposure to light). Usually, a sophisticated technique like transmission electron microscopy (TEM) is utilized to study the nature of nanomaterials [63, 64]. As GO is anticipated to be affected by exposure to the electron beam, care is required for a careful interpretation of TEM observations. TEM image of the as-prepared sample GO-65C and rGO-60 min is shown in Fig. 2a and b, where wrinkles and folds are evident in GO-65C and transparent sheets (due to few layers of sheet) in rGO-60 min which has less crumpling and folds in comparison to GO. To quantify the defects in GO [63] and study the role of the electron beam, we obtained selective area electron diffraction (SAED) of GO-65C (see Fig. 2c). We allowed exposure of electronic beam to the as-prepared GO for 5 min and observed its SAED pattern (see Fig. 2d). It was found that the diffused rings in Fig. 2c evolves into bright spots, which indicates crystalline behavior and restoration of the π bond (suggesting a reduction of GO). In order to further explore the reduction through electron beam, we exposed the sample for another 5 min and measured its SAED pattern (Fig. 2e). We found that the less bright spots in Fig. 2d are evolving into very bright spots in Fig. 2e which signify a higher degree of reduction in GO sample and formation of rGO. Therefore, it is worth mentioning that while analyzing TEM data for GO and its derivatives, the overall exposure to the electron beam is crucial and must be kept in consideration.

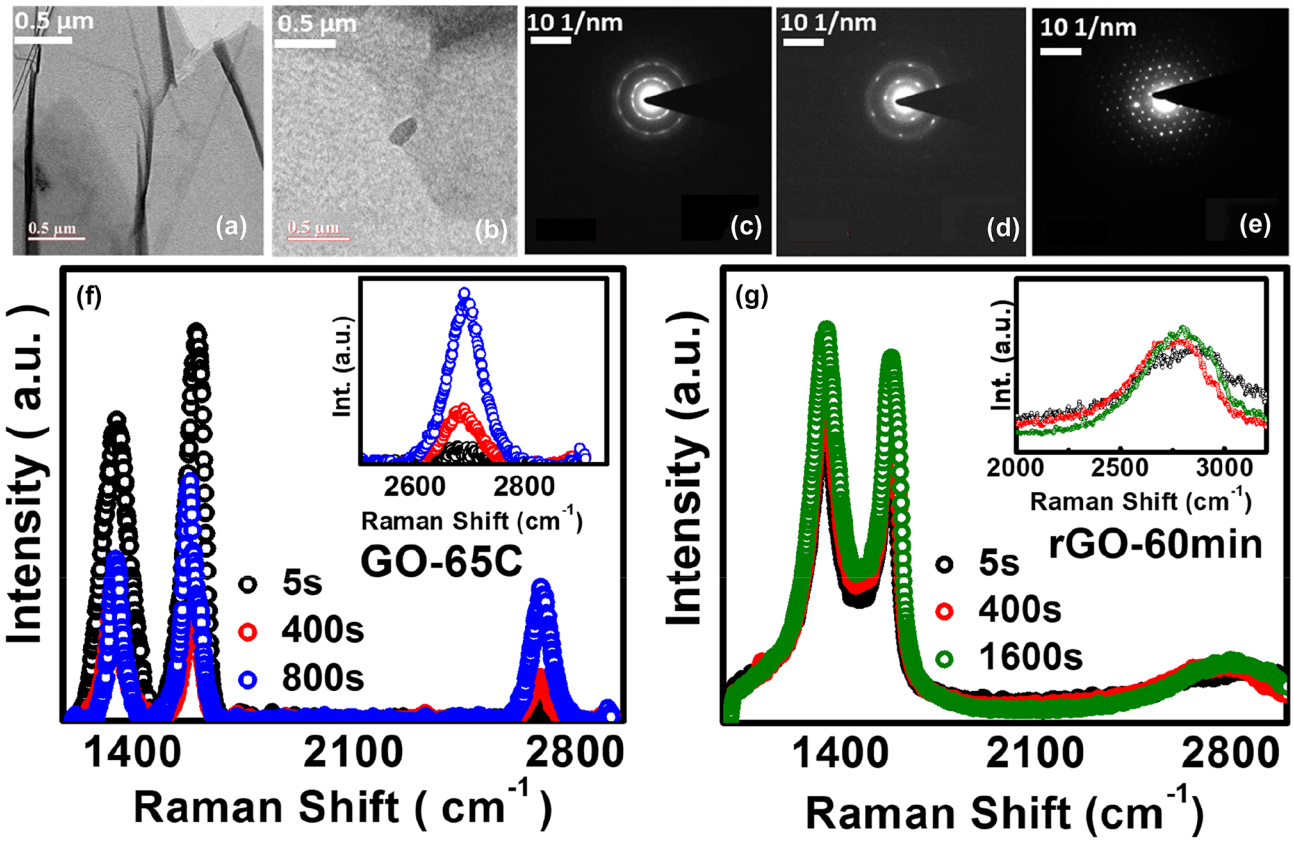

Fig. 2 **a** TEM image of the as-prepared GO-65C sample, **b** TEM image of the as-prepared rGO-60 min sample, **c** Selected area electron diffraction (SAED) pattern of the sample (**a**), **d** after exposure of electron beam for 5 min, **e** after exposure of electron beam for total of 10 min, **f** Raman spectra of GO-65C sample on a glass substrate after laser exposure (inset contains the magnified 2D peak), **g** Raman spectra of rGO-60 min after laser exposure (inset contains the magnified 2D peak)

3.3 Interaction of laser light with GO and rGO during raman spectroscopy

Raman spectroscopy is a niche non-invasive technique for characterizing materials. It has also been extensively used for studying GO and rGO [47, 65–67, 88, 89]. However, exposure of laser light to GO in Raman spectroscopy for longer duration can lead to its reduction. To verify this, we exposed GO and rGO samples for different times (based on accumulation time and the total number of accumulations) during data acquisition using a laser operating at 514.5 nm and 30 mW (at magnification 50X in our setup). Figure 2f shows the Raman spectra of the GO sample which contains three bands D, G and 2D band centered at the position of 1340 cm^{-1}, 1606 cm^{-1} and 2680 cm^{-1}, respectively. The D band corresponds to defects present in the GO arising from the presence of OFGs and/or the absence of carbon atoms in the hexagonal motifs. Further, the origin of the D band is attributed to the first order, double resonance Raman scattering. The presence of G band marks the in-plane vibration of carbon atoms (E_{2g} vibrational mode) and is related to the second-order, double resonance Raman scattering. Moreover, the 2D band which marks the defect in GO and crystallinity in graphene-based system originates due to second-order triple resonance Raman scattering [68]. With the increase in laser exposure time, we observe a decrease in the I_D/I_G ratio along with a minor shift in the peak position of G band. These observations point to a laser exposure induced reduction [63, 66]. To compare the effect of laser exposure on GO and rGO, we repeated the experiment on the chemically reduced sample rGO-60 min (reduced for 1 h). Figure 2g shows the effect of laser exposure on rGO-60 min. It can be clearly observed that the effect of laser exposure on rGO is much less drastic than on GO. In addition, the G band position in rGO-60 min do not change as it did for GO-65C. Thus, an already reduced sample (which has fewer OFGs as compared to GO) is not affected substantially by laser exposure. It is also worthwhile to point that the I_D/I_G ratio is substantially higher for the chemically reduced rGO compared to the one reduced by laser exposure.

Table 2 and 3 list the exposure time of laser, position of G band, I_D/I_G ratio and the crystallite size (L_a) in Å. Crystallite size has been calculated using Tunistra and Koenig (TK) equation [69] given as:

$$\frac{c(\lambda)}{L_a} = \left(\frac{I_D}{I_G}\right)$$

c (λ) equals 44 Å for laser operating at 514.5 nm. The relation suggests that crystallite size shows an inverse relation with I_D/I_G ratio [69].

Table 2 Comparison between the position of the G band, I_D/I_G ratio and crystallite size of GO after different periods of exposure

Period of Exposure, t (s)	The position of G band (cm^{-1})	I_D/I_G	L_a (Å)
0	1602	1.12	39.2
400	1587	1.07	41.1
800	1575	0.63	69.8

Table 3 Comparison between the position of the G band, I_D/I_G ratio and crystallite size of rGO (reduced for 1 h) after different periods of exposure

Period of Exposure, t (s)	The position of G band (cm^{-1})	I_D/I_G	L_a (Å)
5	1570	1.96	22.4
400	1576	1.79	24.5
1600	1581	1.70	25.8

3.4 Impact of sample details on the UV–visible spectroscopy data for GO

UV–Visible spectrophotometry is another widely used spectroscopic tool to characterize GO. A typical UV–Visible spectrum of GO contains a peak centered at ~224 nm and a shoulder or a hump at ~300 nm. The presence of a peak at 224 nm corresponds to π–π* (C=C) transition, and the shoulder or hump at 300 nm is attributed to n–π* (C=O) transition. UV–Visible spectra of GO (in general) are obtained through dispersing GO in water, followed by ultrasonication. However, literature suggests that the sonicator can elevate the solution temperature which affects the chemical and physical property of GO and its derivatives. A dramatic rise in temperatures leading to localized hot-spots up to 5000 K has been reported [70] in ultrasonicator due to the generation of micro-jets and shock waves [71–73], and a pressure of 20 MPa has been achieved by acoustic cavitations [34]. To develop an understanding of the effect of such a process on GO, we summarize our systematic observations on sample GO-65C in Fig. 3. In our experiment, we explored the effect of prolonged exposure to ultrasonication on dispersed GO. We dispersed 0.1 gm of GO-65C in 200 ml of deionized water (DI water). The dispersed solution was ultrasonicated for up to 260 min, and its spectra were recorded at different sonication time intervals (see Fig. 3b). We found a redshift in the characteristic 224 nm peak and a consequent elimination of the hump with an increase in ultrasonication time. The bandgaps of the samples sonicated for different time intervals are shown in Fig. 3d. For this purpose, bandgaps were estimated using Tauc plots (for an example see inset of Fig. 3c). A bandgap tunability of 3.5–1.6 eV is observed. This attests the reduction of GO concerning sonication time. A schematic comparing the extent

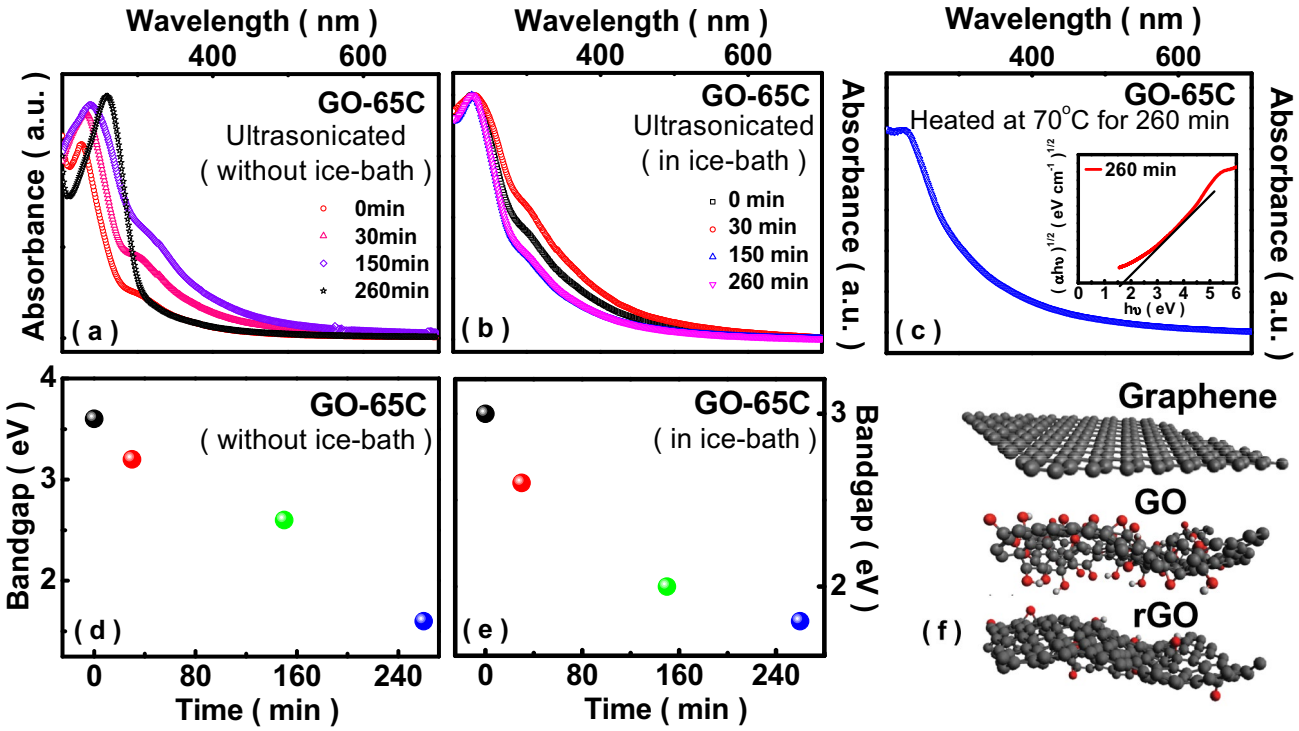

Fig. 3 **a** The UV–Visible spectrum of GO-65C at different time dispersed in water without heating, **b** The UV–Visible spectrum of GO-65C dispersion at a different time (0 min, 30 min, 150 min, 260 min) placed in the cold water bath, **c** The UV–Visible spectrum of GO-65C heated at 70° C for 260 min with its Tauc plot (inset), **d** Bandgap of the treated GO-65C samples in (**a**), **e** Bandgap of the treated GO-65C samples in (**b**) and (**f**) Schematic diagram of graphene, graphene oxide and reduced graphene oxide

of OFGs in GO and related systems is shown in Fig. 3f. It is evident that the GO gets gradually reduced with an increase in ultrasonication time. However, the distinction between the individual contribution of ultrasonication time, heat and sonic waves were not done in Fig. 3d. Typically, ultrasonication of GO solution is a regular process, done before a host of experiments to form a homogenous solution. We assume that this process also deteriorates GO as the thermal energy created is responsible for its reduction during the sonication process. To study separately the impact of the thermal energy and the sonic waves for different sonication times on the reduction of GO, two different protocols were followed. To begin with, DI water was taken in a beaker and was sonicated for 260 min uninterrupted. A rise in temperature of the DI water was noted as 70° C in comparison at 0 min at room temperature. In the first protocol for the demonstration of thermal energy reduction, we heated the GO dispersion (for the sample GO-65C) at the same temperature of 70° C for 260 min and its corresponding UV–Vis spectra were obtained as shown in Fig. 3c. The reduction was anticipated due to heating which is shown with the disappearance of n–π* (C=O) transition, and a resulting bandgap of 1.6 eV has been calculated from the Tauc plot. In the second protocol, the experiment was performed using the ultrasonicator bath for the period of 0–260 min but without letting the temperature of the solution increase (with the help of an ice-bath; see Fig. 3e). This was done to see the exclusive effect of sonic waves on the reduction of GO. It is evident from the Fig. 3b that even after the sonication time of 260 min, n–π* (C=O) transition positioned near to 300 nm did not vanish, and there is no change in the peak position for π–π* (C=C) transition (fixed near 224 nm for all). However, we observed the decrease in the bandgap with increasing sonication time as sonic waves are strong waves that shear the GO flakes and removes the attached functional groups and reduce them to rGO. But the presence and the absence of peak near n–π* transition in Fig. 3b, c, respectively, suggest that C=O groups get readily affected by the direct heating. This experiment suggests that in order to preserve the maximum information of the oxygen functional group contents in GO, ultrasonication can be done in an ice-bath with minimal time duration to form the homogenous solution**.** Figure 3e shows the corresponding variation in the bandgap in the range of 1.8–3.0 eV.

3.5 Photoluminescence (PL) spectra based on the differences in the GO storage and its reduction

Pure graphene is a zero-bandgap semi-metal [87] which do not respond to photoluminescence (PL) excitations. Its valence and conduction bands touch each other at Dirac

points and form a conical surface in the momentum space (see Fig. 4a). However, as we oxidize the graphene sheet, its π electron network i.e., the sp^2 carbons start converting into sp^3 state due to the OFGs attachment to the carbon sheet as a result of electron transfer from carbon to oxygen (see Fig. 4a). This causes a shift in the highest occupied molecular orbital (HOMO) energy level and the energy bandgap now attains a non-zero value. In such a system, that contains mixed hybridisation states (sp^2 and sp^3), the optoelectronic property is taken care of mainly by the π states from the sp^2 component [74]. Such a system responds to the PL excitation energy and shows an emission following the radiative recombination of the electron–hole pairs in the sp^2 domain [75]. A detailed analysis of energy bandgap tuning with the degree of oxidation has already been reported by us [76]. In this experiment, we see the sensitivity of GO solution toward the PL measurement. We prepared GO dispersions with different degrees of oxidation starting with GO-65C. Figure 4b shows the PL of freshly prepared GO-65C; Fig. 4c shows PL of GO which was kept at room temperature under normal white light (WL) of room (no direct exposure) for a month and is marked as GO_{WL}; Fig. 4d shows thermally reduced (TR) GO at 70 °C for 260 min (labeled GO_{TR}). In each case, 0.1 g of GO flake was dispersed in 200 ml of DI water where GO got exfoliated after 10 min and was homogenized with stirring. 2 ml solution in each case was taken in a quartz cuvette of path length 1 cm, and their PL spectra were recorded. PL emission lines in the visible range from 400 to 800 nm and were excited in the range of 340–490 nm. GO, GO_{WL} and GO_{TR} to demonstrate excitation dependence emission with red-shifted PL spectra [77–79] thus, violating Kasha's rule. Most emission has taken in a range of 545–560 nm (Fig. 4b), 576–589 nm (Fig. 4c) and 570–587 nm (Fig. 4d) which corresponds to the bandgap range of 2.27–2.21 eV (Fig. 4b), 2.15–2.10 eV (Fig. 4c) and 2.17–2.11 eV (Fig. 4d). We see that the bandgap of GO is higher than GO_{WL} and GO_{TR}. Pure graphene has a zero-bandgap and as the OFGs start attaching to the graphene plane, the bandgap starts opening. GO being highly oxidized shows the maximum bandgap in comparison to GO_{WL} and GO_{TR}. However, GO_{WL} and GO_{TR} have comparable bandgaps. It can be explained as, fresh GO being sensitive to the outer atmosphere, and gets reduced after a month even under normal white light at room temperature and its bandgap comes close to the thermally reduced GO. The inset panels in Fig. 4b and c in each case shows the GO solution under normal white light and UV chamber, respectively. UV chamber excitation wavelength ($\lambda_{ex} = 365$ nm) resulted in a blue emission for case Fig. 4b, d and moss green for Fig. 4c. Some OFGs and the C = C present in GO is considered to be the fluorophores responsible for the emission spectra [80]. GO stoichiometry varies with the variation in synthesis protocols, preservation technique

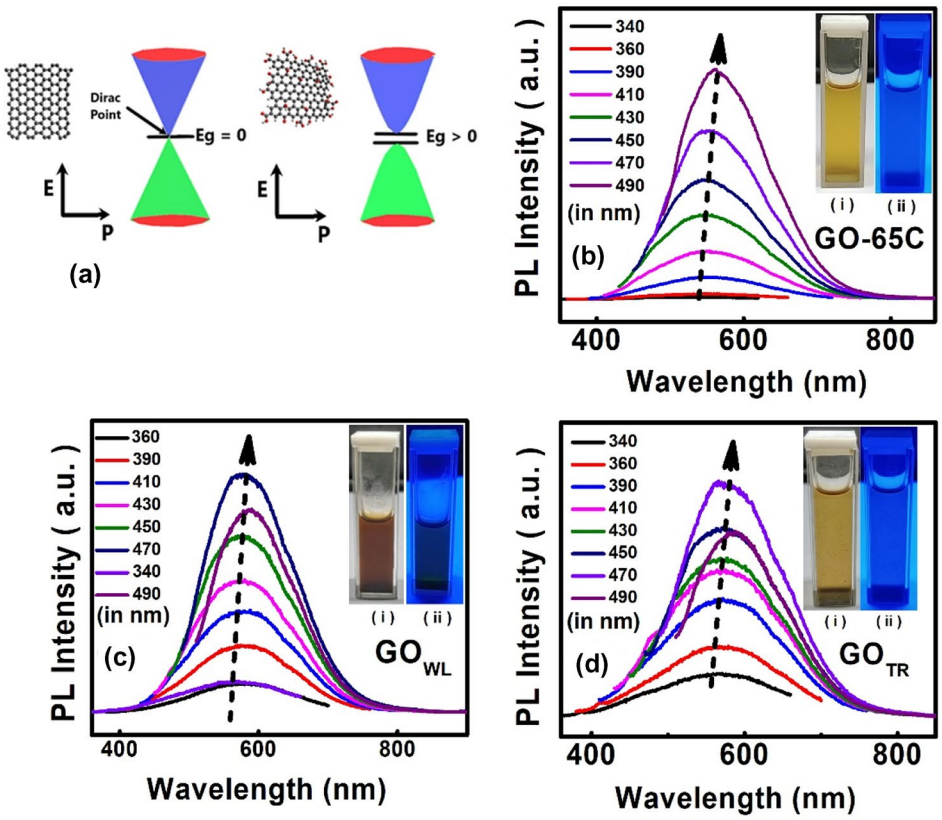

Fig. 4 **a** Schematic representation of bandgap opening in GO as OFGs are attached to the carbon sheet, **b** PL spectra of freshly prepared GO, **c** PL spectra of GO kept for a month at room temperature under white light and **d** PL spectra of thermally reduced GO reduced at 70° C for 260 min

of the sample, the environment of the PL experiment, time elapsed between the freshly prepared GO and the emission taken and, on the nature, and the density of the fluorophores present in different concentration of GO solutions.

3.6 Nuances with the X-ray photoelectron spectroscopy (XPS) of GO

XPS is another widely used experimental tool to get quantitative information on GO. However, the study of the effect of X-ray exposure on GO is missing in the literature of GO. We, therefore, exposed GO to X-rays for the three-line scans (thereby increasing exposure time) in the same region under the same condition and observed its spectra. We obtained the C1s spectra of GO and represented it in black color (see Fig. 5a) [47]. The starting spectra of GO have two major peaks centered at 248.2 eV and 286.4 eV, where 284.2 eV belongs to graphitic domains present in the system, and OFGs can be traced out from the peak at 286.4 eV [6, 14, 31, 47]. Repeated scan at the same place has shown a sharp decrease in a peak at 286.4 eV. This signifies a reduction of GO sample as there is a clear loss in the area of 286.4 eV which signifies OFGs. The observed spectrum after three-line scans (and a considerably larger exposure to X-ray beam) is shown in red color (see Fig. 5a). This reduction of OFGs is related to photo-reduction [65, 81] (as discussed in the TEM section) and appears to be the most prominent reason behind the decrease in the peak at 286.4 eV. Photolysis is defined as the process in which light of a particular wavelength gets absorbed to oxygen functional groups by molecular resonance [81]. The adsorbed light contains enough energy which led to localized heating and thus helps in the bond-breaking of oxygen functional group. In our case (graphene oxide), functional groups such as C–O–C, –COOH and –OH are prominent and likely to get dissociated. This suggests the need for minimum exposure to measuring probe beam in an XPS measurement while characterizing GO and related materials. In accordance with the above observation, faster scan rates were used for the other samples. Figure 5b shows the C1s peak of GO and rGO with different degrees of oxidation to confirm the reduction reported in Fig. 5a. One can note the significantly larger contribution from OFGs in the case of GO-65C compared to GO-50C, rGO-01 min and rGO-80 min as summarized in Table 4. Due to a slower acquisition rate in GO-65C, the raw data have more data points, and the enhanced noise could be surmised to the ensuing reduction process.

3.7 Interpretation of atomic force microscopy (AFM) of GO

AFM study reveals the morphology (wrinkles and folds) of GO sample when dispersed in low concentration at different

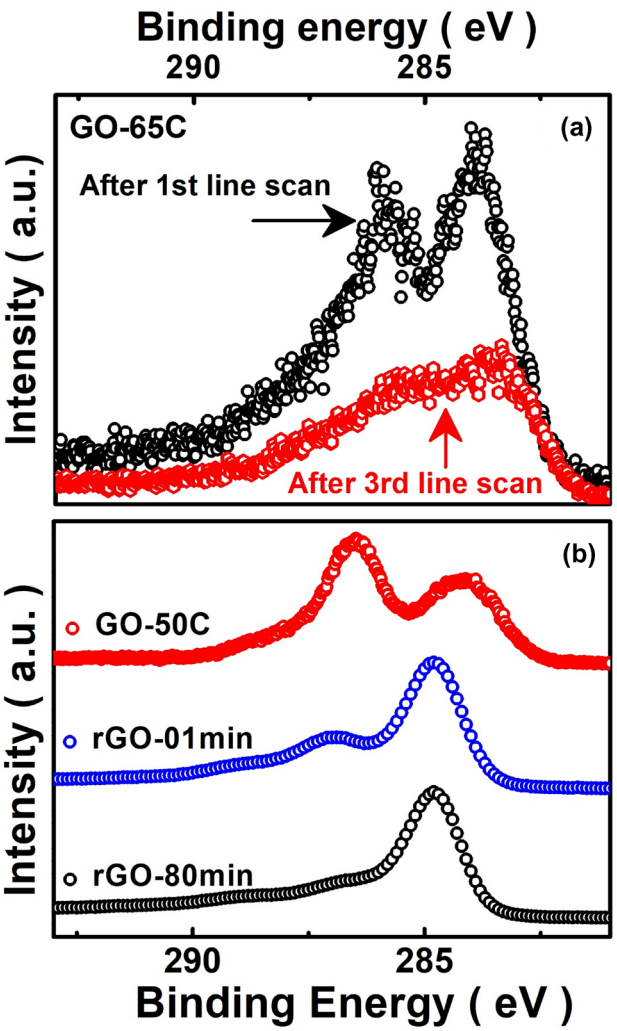

Fig. 5 **a** XPS C1s spectra of graphene oxide (GO-65C) obtained after first and third line scans. **b** Comparison of XPS C1s spectra for GO-50C, rGO-1 min and rGO-80 min

length scales. However, when the dispersion is changed, or the sonication time is varied or the spin-coating rate is altered while preparing dispersed GO solution, the morphology of the sample changes. In this aspect, we, therefore, prepared two sets of samples dispersed in the same organic solvent but spin-coated at different rates. We begin our sample preparation by dispersing 10 mg of GO into 40 ml of DI water. The as-prepared solution was spin-coated at 5000 rpm on SiO_2/Si substrate followed by heating at 80° C for 1 h. Another sample set was prepared at low rpm (800 rpm) using spin-coater on SiO_2/Si substrate followed with heating at 80° C for 1 h. Before spin-coating the SiO_2/Si substrate, it was cleaned using piranha cleaning followed by rinsing in DI water, acetone and ethanol. All the measurements were done in non-contact mode. For the first batch of samples dispersed at 5000 rpm and ultrasonicated for 15 min corresponding AFM images were marked in Fig. 6a, b, c and d.

Table 4 Content of oxygen functional groups in GO and rGO (in %)

S. no	Samples	283.9/284.1 eV (C = C)	284.9 eV (C–C)	286.3 eV (C–O)	288.3 eV (O–C–O/C = O)	285.8 eV (C–OH)	Total % of oxygen
1	GO-65C	40.6	17.6	21.8	13.4	6.6	41.8
2	GO-50C	44.0	17.1	24.7	7.9	6.3	38.9
3	rGO-01 min	42.6	17.6	20.2	13.0	6.6	39.8
4	rGO-80 min	53.7	13.9	13.9	12.9	5.6	32.4

The second batch of the sample with 5 min ultrasonication and the spin-coating rate at 800 rpm was marked in Fig. 6e, f, g and h. It was observed that the film prepared at higher rpm has a thickness of 3–4 nm (see Fig. S1a–o), and a lateral dimension of 800–900 nm (for details see Fig. S1b–p). Also, wrinkles are observed (evident from Fig. S1i–o). However, at lower rpm, we observed lateral dimension of 10 µm in GO film at more than 10 layers that is prominent (see Fig. S1q–y), and its wrinkles/ folding in thickness changes from 4 to more than 30 nm (see Fig. S1r–z).

4 Conclusion

We studied in detail the effect of protocols used during synthesis and characterization of GO and its derivatives and found an extreme sensitivity to these protocols. Based on the observations reported in the paper, appropriate care and caution are desirable while handling these materials for making a judicious choice for various promising applications. In particular, we have the following key suggestions: (a) during the analysis of XRD data, the observed peak position depends on the degree of oxidation which in turn may be affected by exact details of storage (including exposure to light and humidity and temperature variations in the ambient) and sample preparation for conducting powder XRD measurement, (b) during TEM and SAED experiments, the exposure to electron beam potentially modifies GO and the analysis of the data must factor this in, (c) the exposure to laser light during Raman spectroscopy should be monitored for any resulting changes in the location of D- and G-peaks, (d) an appropriate care is required during the preparation of samples for UV–Visible absorption studies. An ice-bath is recommended during the ultrasonication process while dispersing GO in the solvent, (e) the PL spectra is sensitive to the sample storage protocols, and a proper account must be made of a possible reduction which may lead to variation in the density of fluorophores, (f) during XPS measurements in GO and rGO, the exposure time to X-rays plays a crucial role and must be kept to a minimum to access the true composition of the sample, (g) the AFM study reveals the morphology of GO sample dispersion, but, the morphology changes with the change in the sonication time and the spin-coating rates, and (h) it is recommended to store nominally reduced

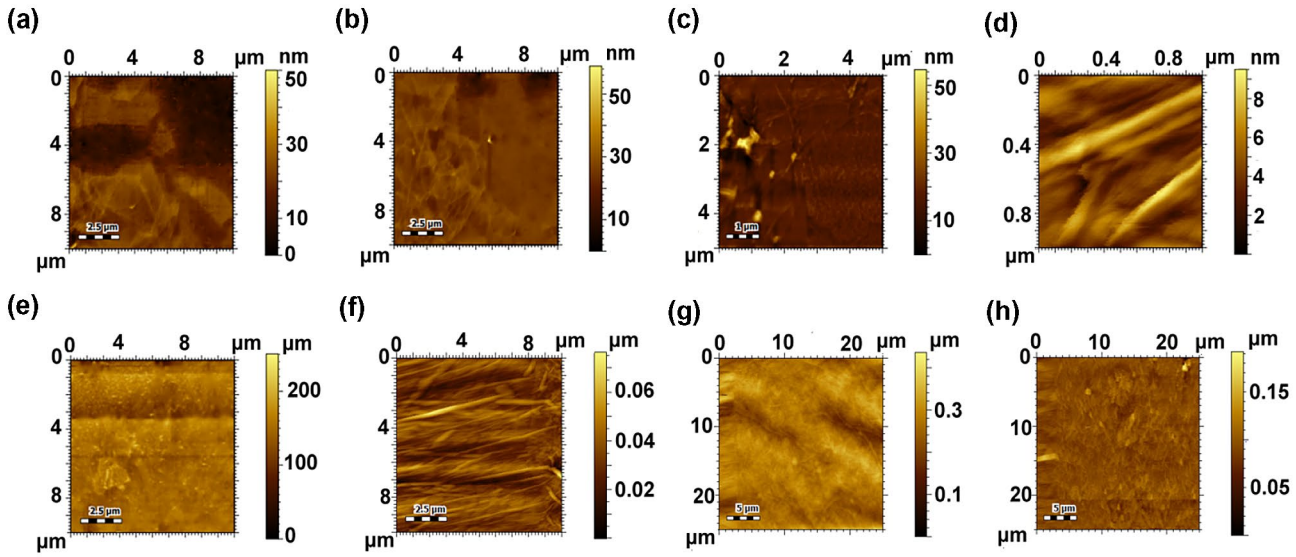

Fig. 6 AFM image of GO sample drop casted on a glass substrate and spin-coated at different rotational speeds of 5000 rpm (panels **a**-**d**) and 800 rpm (panels **e**–**g**)

rGO (say rGO-1 min) instead of GO. To conclude, GO and its derivatives have a tremendous application potential, but significant care is required in the protocols used during their synthesis and characterization for achieving the objectives reliably. The present work elucidates the variability in physical properties of GO depending on the details of the protocols used during synthesis and characterization. This can also help establish best practices in GO synthesis and characterization protocols for addressing the exact functional requirements related to an end application.

Supplementary Information The online version contains supplementary material available at https://doi.org/10.1007/s00339-021-04734-z.

Acknowledgements AS thanks support from the University Grants Commission (UGC), India for financial support. The authors thank MHRD, Government of India for financial support.

References

1. S. Obata, K. Saiki, T. Taniguchi, T. Ihara, Y. Kitamura, Y. Matsumoto, Graphene oxide: a fertile nanosheet for various applications. J. Phys. Soc. Japan **84**, 1–18 (2015)
2. S.I. Abdullah, M.N.M. Ansari, Mechanical properties of graphene oxide (GO)/epoxy composites. HBRC J. **11**, 151–156 (2015)
3. Z. Liu, Y. Wang, X. Zhang, Y. Xu, Y. Chen, J. Tian, Nonlinear optical ptoperties of graphene oxide in nanosecond and picosecond regimes. Appl. Phys. Lett. **94**, 021902 (2009)
4. X. Wang, J. Zhang, X. Mei, J. Miao, X. Wang, Laser-induced forward transfer of graphene oxide. Appl. Phys. A **127**, 207 (2021)
5. S. Mittal, V. Kumar, N. Dhiman, L.K.S. Chauhan, R. Pasricha, A.K. Pandey, Physico-chemical properties based differential toxicity of graphene oxide/reduced graphene oxide in human lung cells mediated through oxidative stress. Sci. Rep. **6**, 39548 (2016)
6. D.C. Marcano, D.V. Kosynkin, J.M. Berlin, A. Sinitskii, Z. Sun, A. Slesarev, L.B. Alemany, W. Lu, J.M. Tour, Improved synthesis of graphene oxide. ACS Nano **4**, 4806–4814 (2010)
7. V.A. Smirnov, N.N. Denisov, M.V. Alfimov, Photochemical reduction of graphite oxide. Nanotechnologies Russ. **8**, 1–22 (2013)
8. M. Wang, L.D. Duong, N.T. Mai, S. Kim, Y. Kim, H. Seo, Y.C. Kim, W. Jang, Y. Lee, J. Suhr, J. Do Nam, All-solid-state reduced graphene oxide supercapacitor with large volumetric capacitance and ultralong stability prepared by electrophoretic deposition method. ACS Appl. Mater. Interfaces **7**, 1348–1354 (2015)
9. B. Li, H. Cao, ZnO@ graphene composite with enhanced performance for the removal of dye from water. J. Mater. Chem. **21**, 3346–3349 (2011)
10. Z. Liu, J.T. Robinson, X. Sun, H. Dai, PEGylated nanographene oxide for delivery of water-insoluble cancer drugs. J. Am. Chem. Soc. **130**, 10876–10877 (2008)
11. T. Al-Gahouari, P. Sayyad, G. Bodkhe, N. Ingle, M. Mahadik, S. Shirsat, M. Shirsat, Controlling reduction degree of graphene oxide-based electrode for improving the sensing performance toward heavy metal ions. Appl. Phys. A **127**, 170 (2021)
12. R. Sitko, E. Turek, B. Zawisza, E. Malicka, E. Talik, J. Heimann, A. Gagor, B. Feist, R. Wrzalik, Adsorption of divalent metal ions from aqueous solutions using graphene oxide. Dalt. Trans. **42**(16), 5682–5689 (2013)
13. X. Li, W. Xu, M. Tang, L. Zhou, B. Zhu, S. Zhu, J. Zhu, Graphene oxide-based efficient and scalable solar desalination under one sun with a confined 2D water path. Proc. Natl. Acad. Sci. U. S. A. **113**, 13953–13958 (2016)
14. O. Akhavan, E. Ghaderi, Toxicity of graphene and graphene oxide nanowalls against bacteria. ACS Nano **4**, 5731–5736 (2010)
15. O. Akhavan, E. Ghaderi, S. Aghayee, Y. Fereydooni, A. Talebi, The use of a glucose- reduced graphene oxide suspension for photothermal cancer therapy. J. Mater. Chem. **2**, 13773–13781 (2012)
16. O. Akhavan, E. Ghaderi, E. Abouei, S. Hatamie, E. Ghasemi, Accelerated differentiation of neural stem cells intoneurons on ginseng-reduced graphene oxide sheets. Carbon **66**, 395–406 (2014)
17. X. Wang, M. Yu, W. Zhang, B. Zhang, L. Dong, Synthesis and microwave absorption properties of graphene/nickel composite materials. Appl. Phys. A **118**, 1053–1058 (2015)
18. M. Goumri, J.W. Venturini, A. Bakour, M. Khenfouch, M. Baitoul, Tuning the luminescence and optical properties of graphene oxide and reduced graphene oxide functionnalized with PVA. Appl. Phys. A **122**, 212 (2016)
19. N. Bano, I. Hussain, A.M. El-Naggar, A.A. Albassam, Reduced graphene oxide nanocomposites for optoelectronics applications. Appl. Phys. A **125**, 215 (2019)
20. M. Sarno, A. Senatore, C. Cirillo, V. Petrone, P. Ciambelli, Oil lubricant tribological behaviour improvement through dispersion of few layer graphene oxide. J. Nanosci. Nanotechnol. **14**, 4960–4968 (2014)
21. B.C. Brodie, On the atomic weight of graphite. Phil. Trans. R. Soc. L. **149**, 249–259 (1859)
22. F. Gottschalk, Beiträge zur kenntniss der graphitsäure. J. Prakt. Chem. **95**, 321–350 (1865)
23. L. Staudenmaier, Verfahrenzur darstellung der graphitslure. Ber. Dtsch. Chem. Ges. **31**, 1481–1487 (1898)
24. M. Berthelot, Recherches sur lesétats du carbonne. Ann. Chim. Phys. **19**, 391–417 (1870)
25. W. Luzi, Beiträge zur kenntnis des graphitkohlenstoffs. Z. Naturwiss **64**, 224–269 (1891)
26. G. Charpy, Sur la formation de l'oxyde graphitique et la définition du graphite. C. R. Hebd. Seances Acad. Sci. **148**, 920–923 (1909)
27. H. Hamdi, Zur kenntnis der kolloidchemischen eigenschaften des humus disperscoidchemische beobachtungen graphitoxid. Kolloid Beihefte **54**, 554–643 (1942)
28. E. Weinschenk, Über den graphitkohlenstoff und die gegenseitigen beziehungenzwischen graphit Graphitit and Graphitoxid. Z. Krist. **28**, 291–304 (1897)
29. V. Kohlschutter, P. Haenni, Zur kenntnis des graphitischen kohlenstoffs und der graphitsäure. Z. Anorg. Chem. **105**, 121–144 (1919)
30. W.S. Hummers Jr., R.E. Offeman, Preparation of graphitic oxide. J. Am. Chem. Soc. **80**, 1339–1339 (1958)
31. M. Hirata, T. Gotou, S. Horiuchi, M. Fujiwara, M. Ohba, Thin-film particles of graphite oxide 1: high yield synthesis and flexibility of the particles. Carbon **42**, 2929–2937 (2004)
32. H.L. Poh, F. Šaněk, A. Ambrosi, G. Zhao, Z. Sofer, M. Pumera, Graphenes prepared by staudenmaier, hofmann and hummers methods with consequent thermal exfoliation exhibit very different electrochemical properties. Nanoscale **4**, 3515–3522 (2012)
33. D.R. Dreyer, S. Park, C.W. Bielawski, R.S. Ruoff, The chemistry of grapheme oxide. Chem. Soc. Rev. **39**, 228–240 (2010)
34. C. Tao, J. Wang, S. Qin, Y. Lv, Y. Long, H. Zhu, Z. Jiang, Fabrication of pH-sensitive graphene oxide–drug supramolecular hydrogels as controlled release systems. J. Mater. Chem. **22**, 24856–24861 (2012)
35. D. Li, M.B. Müller, S. Gilje, R.B. Kaner, G.G. Wallace, Processable aqueous dispersions of graphene nanosheets. Nat. Nanotechnol. **3**, 101–105 (2008)
36. S. Peng, X. Fan, S. Li, J. Zhang, Green synthesis and characterization of graphite oxide by orthogonal experiment. J. Chil. Chem. Soc. **58**, 2213–2217 (2013)

37. H.J. Shin, K.K. Kim, A. Benayad, S.M. Yoon, H.K. Park, I.S. Jung, M.H. Jin, H.K. Jeong, J.M. Kim, J.Y. Choi, Y.H. Lee, Efficient reduction of graphite oxide by sodium borohydride and its effect on electrical conductance. Adv. Funct. Mater. **19**, 1987–1992 (2009)
38. Y. Zhou, Q. Bao, L.A.L. Tang, Y. Zhong, K.P. Loh, Hydrothermal dehydration for the "green" reduction of exfoliated graphene oxide to graphene and demonstration of tunable optical limiting properties. Chem. Mater. **21**, 2950–2956 (2009)
39. J.H. Chu, J. Kwak, S.D. Kim, M.J. Lee, J.J. Kim, S.D. Park, J.K. Choi, G.H. Ryu, K. Park, S.Y. Kim, J.H. Kim, Z. Lee, Y.W. Kim, S.Y. Kwon, Monolithic graphene oxide sheets with controllable composition. Nat. Commun. **5**, 3383 (2014)
40. J. Shen, Y. Hu, M. Shi, X. Lu, C. Qin, C. Li, M. Ye, Fast and facile preparation of graphene oxide and reduced graphene oxide nanoplatelets. Chem. Mater. **21**, 3514–3520 (2009)
41. S. Eigler, M. Enzelberger-Heim, S. Grimm, P. Hofmann, W. Kroener, A. Geworski, C. Dotzer, M. Röckert, J. Xiao, C. Papp, O. Lytken, H.P. Steinrück, P. Müller, A. Hirsch, Wet chemical synthesis of graphene. Adv. Mater. **25**, 3583–3587 (2013)
42. N.M. Huang, H.N. Lim, C.H. Chia, M.A. Yarmo, M.R. Muhamad, Simple room-temperature preparation of high-yield large area graphene oxide. Int. J. Nanomed. **6**, 3443–3448 (2011)
43. H.A. Becerril, J. Mao, Z. Liu, R.R.M. Stoltenberg, Z. Bao, Y. Chen, Evaluation of solution-processed reduced graphene oxide films as transparent conductors. ACS Nano **2**, 463–470 (2008)
44. L. Peng, Z. Xu, Z. Liu, Y. Wei, H. Sun, Z. Li, X. Zhao, C. Gao, An iron-based green approach to 1-h production of single-layer graphene oxide. Nat. Commun. **6**, 5716 (2015)
45. S. Stankovich, D.A. Dikin, R.D. Piner, K.A. Kohlhaas, A. Kleinhammes, Y. Jia, Y. Wu, S.B.T. Nguyen, R.S. Ruoff, Synthesis of graphene-based nanosheets via chemical reduction of exfoliated graphite oxide. Carbon **45**, 1558–1565 (2007)
46. P.G. Ren, D.X. Yan, X. Ji, T. Chen, Z.M. Li, Temperature dependence of graphene oxide reduced by hydrazine hydrate. Nanotechnology **22**, 055705 (2011)
47. P. Ranjan, S. Agrawal, A. Sinha, T.R. Rao, J. Balakrishnan, A.D. Thakur, A low-cost non-explosive synthesis of graphene oxide for scalable applications. Sci. Rep. **8**, 12007 (2018)
48. F.T. Johra, J.W. Lee, W.G. Jung, Facile and safe graphene preparation on solution based platform. J. Ind. Eng. Chem. **20**, 2883–2887 (2014)
49. L. Zhang, J. Xia, Q. Zhao, L. Liu, Z. Zhang, Functional graphene oxide as a nanocarrier for controlled loading and targeted delivery of mixed anticancer drugs. Small **6**, 537–544 (2010)
50. O. Akhavan, Photocatalytic reduction of graphene oxides hybridized by ZnO nanoparticles in ethanol. Carbon **49**, 11–18 (2011)
51. D.W. Chang, H.J. Choi, I.Y. Jeon, J.M. Seo, L. Dai, J.B. Baek, Solvent-free mechanochemical reduction of graphene oxide. Carbon **77**, 501–507 (2014)
52. S. Pei, J. Zhao, J. Du, W. Ren, H.M. Cheng, Direct reduction of graphene oxide films into highly conductive and flexible graphene films by hydrohalic acids. Carbon **48**, 4466–4474 (2010)
53. D. He, Z. Kou, Y. Xiong, K. Cheng, X. Chen, M. Pan, S. Mu, Simultaneous sulfonation and reduction of graphene oxide as highly efficient supports for metal nanocatalysts. Carbon **66**, 312–319 (2014)
54. Y. Matsumoto, M. Koinuma, S.Y. Kim, Y. Watanabe, T. Taniguchi, K. Hatakeyama, H. Tateishi, S. Ida, Simple photoreduction of graphene oxide nanosheet under mild conditions. ACS Appl. Mater. Interfaces **2**, 3461–3466 (2010)
55. O. Akhavan, E. Ghaderi, S.A. Shirazian, R. Rahighi, Rolled graphene oxide foams as three-dimensional scaffolds for growth of neural fibers using electrical stimulation of stem cells. Carbon **97**, 71–77 (2016)
56. X. Chen, D. Meng, B. Wang, B.W. Li, W. Li, C.W. Bielawski, R.S. Ruoff, Rapid thermal decomposition of confined graphene oxide films in air. Carbon **101**, 71–76 (2016)
57. D. Yang, A. Velamakanni, G. Bozoklu, S. Park, M. Stoller, R.D. Piner, S. Stankovich, I. Jung, D.A. Field, C.A. Ventrice, R.S. Ruoff, Chemical analysis of graphene oxide films after heat and chemical treatments by X-ray photoelectron and micro-raman spectroscopy. Carbon **47**, 145–152 (2009)
58. S. Drewniak, R. Muzyka, A. Stolarczyk, T. Pustelny, M. Kotyczka-Morańska, M. Setkiewicz, Studies of reduced graphene oxide and graphite oxide in the aspect of their possible application in gas sensors. Sensors **16**, 103 (2016)
59. G. Sobon, J. Sotor, J. Jagiello, R. Kozinski, M. Zdrojek, M. Holdynski, P. Paletko, J. Boguslawski, L. Lipinska, K.M. Abramski, Graphene oxide vs. reduced graphene oxide as saturable absorbers for Er-doped passively mode-locked fiber laser. Opt. Express **20**, 19463–19473 (2012)
60. D. Voiry, J. Yang, J. Kupferberg, R. Fullon, C. Lee, H.Y. Jeong, H.S. Shin, M. Chhowalla, High-quality graphene via microwave reduction of solution-exfoliated graphene oxide. Science **353**, 1413–1416 (2016)
61. S. Abdolhosseinzadeh, H. Asgharzadeh, H.S. Kim, Fast and fully-scalable synthesis of reduced graphene oxide. Sci. Rep. **5**, 10160 (2015)
62. A.M. Dimiev, L.B. Alemany, J.M. Tour, Graphene oxide: origin of acidity, its INSTABILITY in water, and a new dynamic structural model. ACS Nano **7**, 576–588 (2013)
63. K. Krishnamoorthy, M. Veerapandian, K. Yun, S.J. Kim, The chemical and structural analysis of graphene oxide with different degrees of oxidation. Carbon **53**, 38–49 (2013)
64. H. Feng, R. Cheng, X. Zhao, X. Duan, J. Li, A low-temperature method to produce highly reduced graphene oxide. Nat. Commun. **4**, 1539 (2013)
65. D.A. Sokolov, K.R. Shepperd, T.M. Orlando, Formation of graphene features from direct laser-induced reduction of graphite oxide. J. Phys. Chem. Lett. **1**, 2633–2636 (2010)
66. A.C. Ferrari, J.C. Meyer, V. Scardaci, C. Casiraghi, M. Lazzeri, F. Mauri, S. Piscanec, D. Jiang, K.S. Novoselov, S. Roth, A.K. Geim, Raman spectrum of graphene and graphene layers. Phys. Rev. Lett. **97**, 187401 (2006)
67. K. Krishnamoorthy, M. Veerapandian, R. Mohan, S. Kim, Investigation of raman and photoluminescence studies of reduced graphene oxide sheets. Appl. Phys. A **106**, 501–506 (2012)
68. J.J. Zhang, H. Yang, G. Shen, P. Cheng, J.J. Zhang, S. Guo, Reduction of graphene oxide via L-ascorbic acid. Chem. Commun. **46**, 1112–1114 (2010)
69. F. Tuinstra, J.L. Koenig, Raman spectrum of graphite. J. Chem. Phys. **53**, 1126 (1970)
70. K.S. Suslick, N.C. Eddingsaas, D.J. Flannigan, S.D. Hopkins, H. Xu, Extreme conditions during multibubble cavitation: sonoluminescence as a spectroscopic probe. Ultrason. Sonochem. **18**, 842–846 (2011)
71. Y. Iida, T. Tuziuti, K. Yasui, T. Kozuka, A. Towata, Protein release from yeast cells as an evaluation method of physical effects in ultrasonic field. Ultrason. Sonochem. **15**, 995–1000 (2008)
72. A. Henglein, M. Gutierrez, Chemical effects of continuous and pulsed ultrasound: a comparative study of polymer degradation and iodide oxidation. J. Phys. Chem. **94**, 5169–5172 (1990)
73. G. Price, P. West, P. Smith, Control of polymer structure using power ultrasound. Ultrason. Sonochem. **1**, S51–S57 (1994)
74. J. Robertson, E.P.O. Reilly, Electronic and atomic structure of amorphous carbon. Phys. Rev. B **35**, 2946–2957 (1987)
75. T. Heitz, C. Godet, J.E. Bouree, B. Drevillon, J.P. Conde, Radiative and nonradiative recombination in polymerlike α−C: h films. Phys. Rev. B **60**, 6045–6052 (1999)

76. A. Sinha, A.D. Thakur, Experimental bandgap tuning of graphene oxide with varying degree of oxidation and reduction. AIP Conf. Proc. **2220**, 140008 (2020)
77. S.K. Cushing, M. Li, F. Huang, N. Wu, Origin of strong excitation wavelength dependent fluorescence of graphene oxide. ACS Nano **8**, 1002–1013 (2014)
78. S.K. Pal, Versatile photoluminescence from graphene and its derivatives. Carbon **88**, 86–112 (2015)
79. Z. Gan, H. Xu, Y. Hao, Mechanism for excitation-dependent photoluminescence from graphene quantum dots and other graphene oxide derivates: consensus, debates and challenges. Nanoscale **8**, 7794 (2016)
80. M. Li, S.K. Cushing, X. Zhou, S. Guo, N. Wu, Fingerprinting photoluminescence of functional groups in graphene oxide. J. Mater. Chem. **22**, 23374–23379 (2012)
81. S. Gilje, S. Dubin, A. Badakhshan, J. Farrar, S.A. Danczyk, R.B. Kaner, Photothermal deoxygenation of graphene oxide for patterning and distributed ignition applications. Adv. Mater. **22**, 419–423 (2010)
82. M. Kashif, E. Jaafar, P. Bhadja, F.W. Low, S.K. Sahari, S. Hussain, F.K. Loong, A. Ahmad, T.S. AlGarni, M. Shafa, H. Asghar, S.A.A. Tamrah, Effect of potassium permanganate on morphological, structural and electro-optical properties of graphene oxide thin films. Arabian J. Chem. **14**, 102953 (2021)
83. M. Rasheed, S. Shihab, O.W. Sabah, An investigation of the structural, electrical and optical properties of graphene-oxide thin films using different solvents. J. Phys. Conf. Ser. **1795**, 012052 (2021)
84. A. Arabpour, S. Dan, H. Hashemipour, Preparation and optimization of novel graphene oxide and adsorption isotherm study of methylene blue. Arabian J. Chem. **14**, 103003 (2021)
85. M.C.F. Costa, V.S. Marangoni, P.R. Ng, H.T.L. Nguyen, A. Carvalho, A.H.C. Neto, Accelerated synthesis of graphene oxide from graphene. Nanomaterials **11**, 551 (2021)
86. J. Kim, J.H. Eum, J. Kang, O. Kwon, H. Kim, D.W. Kim, Tuning the hierarchical pore structure of graphene oxide through dual thermal activation for high-performance supercapacitor. Sci. Rep. **11**, 2063 (2021)
87. G. Lu, K. Yu, Z. Wen, J. Chen, Semiconducting graphene: converting graphene from semimetal to semiconductor. Nanoscale **5**, 1353–1368 (2013)
88. F. Yin, S. Wu, Y. Wang, L. Wu, P. Yuan, X. Wang, Self-assembly of mildly reduced graphene oxide monolayer for enhanced raman scattering. J. Solid State Chem. **237**, 57–63 (2016)
89. M.A. Khaderbad, V. Tjoa, T.Z. Oo, J. Wei, M. Sheri, R. Mangalampalli, V.R. Rao, S.G. Mhaisalkarb, N. Mathews, Facile fabrication of graphene devices through metalloporphyrin induced photocatalytic reduction. RSC Adv. **2**, 4120–4124 (2012)